

## Shot Analysis of Kepler Blazar W2R 1926+42

M. Sasada, S. Mineshige

Department of Astronomy, Graduate School of Science,  
 Kyoto University, Kitashirakawa-Oiwake-cho, Sakyo-ku,  
 Kyoto 606-8502, Japan; sasada@kustastro.kyoto-u.ac.jp

S. Yamada

Department of Physics, Tokyo Metropolitan University,  
 Minami-Osawa 1-1 Hachioji, Tokyo 192-0397, Japan

H. Negoro

Department of Physics, Nihon University, 1-8 Kanda-Surugadai, Chiyoda-ku, Tokyo 101-8308, Japan

Blazars show rapid and violent variabilities, which timescale are often less than a day. We studied intraday variations by applying a “shot analysis” technique to *Kepler* monitoring of blazar W2R 1926+42 in Quarter 14. We obtained a mean profile calculated from 195 rapid variations. The mean profile shows three components; one is a sharp structure distributed within  $\pm 0.1$  day of the peak, and two slow-varying components. This spiky-peak component reflects features of rapid variations directly. The profile of peak component shows an exponential rise and decay of which timescales are different, 0.0416 and 0.0588 day respectively. This component is too sharp to represent a standard function which is often used to express blazar variations. This asymmetric profile at the peak is difficult to be explained by a simple variation of the Doppler factor by changing a geometry of the emitting region. This result indicates that intraday variations arise from a production of high-energy accelerated particles in the jet.

## I. INTRODUCTION

Blazars have relativistic jets whose axes are closely directed along their line of sight [4, 5]. Timescales of brightness variations in blazars are related to sizes of emitting regions and these speeds in relativistic jets. Variations, however, have a variety of timescales from minutes to decades. A power spectrum density (PSD) of blazar shows a power-law distribution, which means that variations of blazars show noise-like behaviors [14]. These various brightness variations in blazars can be happened by a variety of physical situations in relativistic jets. The shorter-timescale variations should be reflected to the physics of inner-emitting regions of a jet. Thus, the study of short-timescale variations is important to investigate the origin of variation in blazar jets.

Blazars show rapid variations having a timescale of less than 1 day. These rapid variations have been reported in wide wavelengths from radio to gamma-ray bands; in the radio [19], optical [7], X-ray [14], and TeV gamma-ray bands [3]. The *Fermi* space telescope has scanned the entire gamma-ray sky every hours, and detected a lot of large-amplitude variations as flares [2, 17, 22]. Detected flares in the gamma-ray band often continued for less than 1 day, and had a variety of shapes, not only a simple rise and decay. We need higher time-resolution and photon-statistics observations to study the detailed feature of rapid variations.

An optical continuous monitoring of blazar W2R 1926+42 with a high time-sampling rate by *Ke-*

*pler* spacecraft [6] detected a lot of rapid variations. Its light curve revealed detailed shapes of numerous variations with large signal-to-noise ratio. We report general features of rapid variations having a timescale less than 1 day by stacking these detected variations, and producing a mean profile of rapid variations, so-called shot analysis. This paper is organized as follows. Details of *Kepler* observation and the way of shot analysis are described in section 2. Observational results and features of the mean profile of rapid variations are reported in section 3. We discuss an origin of rapid variations of the object in section 4, and section 5 gives several concluding remarks.

## II. OBSERVATION AND ANALYSIS

A. *Kepler* data

*Kepler* monitored over a hundred thousand objects in Cygnus regions, and obtained continuous light curves with two timing settings, long (thirty-minute) or short (one-minute) cadences. Blazar W2R 1926+42 is listed in *Kepler* target list. It has been obtained a continuous light curve with the long cadence since Quarter 11. In Quarter 14, the object had been monitored in the short cadence mode for 100 days. We produced the calibrated “SAP\_FLUX” light curve with one-minute time resolution by the automated *Kepler* data processing pipeline [13].

W2R 1926+42 is classified as a low-frequency peaked BL Lac object at  $z = 0.154$  estimated from

two absorption lines [9]. Edelson et al. reported that there were numerous flares with timescales as short as a day in the *Kepler* light curve of Quarter 11 and 12 [10]. The PSD calculated from the light curve showed approximately a power-law distribution, but not simple. It showed a flattening at frequencies below  $7 \times 10^{-5}$  Hz.

### B. Shot analysis

Frequency-domain analyses (e.g. PSD) are not easy to relate with physical mechanisms directly. On the other hand, time-domain analyses keeping phase information of variations can be useful for studying physical mechanisms of variation. We need, however, large photon statistics to study variations with these time-domain analyses, because it is difficult to study detailed features of variations by using only partial data with observational uncertainty. Additionally, observed variations in blazars usually have a variety of shapes. Thus, it is difficult to understand general features of variations in blazars by studying only individual variations.

We apply the light curve of W2R 1926+42 obtained by *Kepler* to a shot analysis proposed by Negoro et al. to study the general features of rapid variations without local features of individual variations, because a mean profile of rapid variations calculated by the shot analysis can be cancelled the local features of individual variations [18]. We analyzed following procedures to make a mean profile; First, we select rapid variations as candidates of shots. Second, we estimate the observational uncertainty in the light curve. Then, we select the rapid variations with four times larger amplitudes than the standard deviation of the observational uncertainty after subtracting the baseline components. We define these variations as shots.

There are two possibilities for varying the observed brightness, intrinsic variation of the object and variation by the observational uncertainty. It is natural that the variation by the observational uncertainty is dominant rather than the intrinsic variation in shorter period, especially in the period between two observing points which lie next to each other. We estimate the standard deviation  $\sigma$  of differences between two neighboring points, and define  $\sigma$  as the observational uncertainty,  $\sigma = 17.15 \text{ count s}^{-1}$ .

Rapid variations are often superposed on long-term variations in light curves of blazars [20]. We approximate a baseline component of rapid variation by a second-order local polynomial fitting to the light curve without the period of the rapid variation. We subtract the calculated baseline component from the light curve, and extract the rapid variation. We detect a shot when the estimated amplitude of extracted rapid variation without the contribution of the baseline component is larger than our threshold,  $> 4\sigma$ .

Additionally, the peak time of the shot is defined at the time of the maximum flux among the period of rapid variation after subtracting the baseline component. We calculate a mean profile of detected shots by stacking with reference to each peak.

## III. RESULTS

Figure 1 shows an optical light curve of the object obtained by *Kepler*. The object showed a violent variability with various timescales ranging from several tens of minutes to over ten days, limiting for the observational uncertainty. In the light curve, there are not only a large-amplitude long-term variation like from JD 2456150 to 2456160, but also a lot of flare-like variations with timescale of hours. These rapid variations existed throughout the entire period of this monitoring. Figure 2 shows examples of rapid variations. We range these rapid variations with reference to the peak times of individual extrema. Figure 2 clearly shows that these variations had a variety of shapes.

We detect 195 shots from the obtained light curve, in pursuance of the definition of shot described in section 2.2. We calculate a mean profile of these detected shots by applying the shot analysis. Upper panel of figure 3 shows the mean profile of shots without the data at peak time, because positive fluctuations of the counts at  $t = 0$  are summed up systematically [18]. There are mainly three components at the mean profile of shots shown in figure 3; a sharp component distributed in  $\pm 0.1$  day of the peak time (component 1), and slow-variable components ranging from  $-0.50$  to  $-0.15$  day and from  $0.10$  to  $0.45$  day (component 2 and 3), respectively. An increase and decrease of flux in component 1 are approximately exponential rise and decay. Additionally, the profile at the peak is changing from rising to decaying phases for approximately ten minutes.

If shot profiles change depending on selected amplitudes of shots, the calculated mean profile does not reflect to general features of shot. We verify whether there is an amplitude dependence to the profile or not. We separate detected shots in three terms based on these amplitudes,  $4-6\sigma$ ,  $6-8\sigma$ , and over  $8\sigma$ , and calculate mean profiles using selected shots. Although calculated profiles show small differences caused by the limited number of shot samples, the mean profile of shots has no clear trend associated with these amplitudes.

We estimate the systematic uncertainty of the obtained mean profile of shots associated with limited sampling by a non-parametric bootstrap approach. First, we resample 195 shots with replacement from detected shots, and calculate a mean profile from the resampled 195 shots. We produce 10000 pseudo mean profiles of shots following this procedure with different resamplings. We normalize an average of each

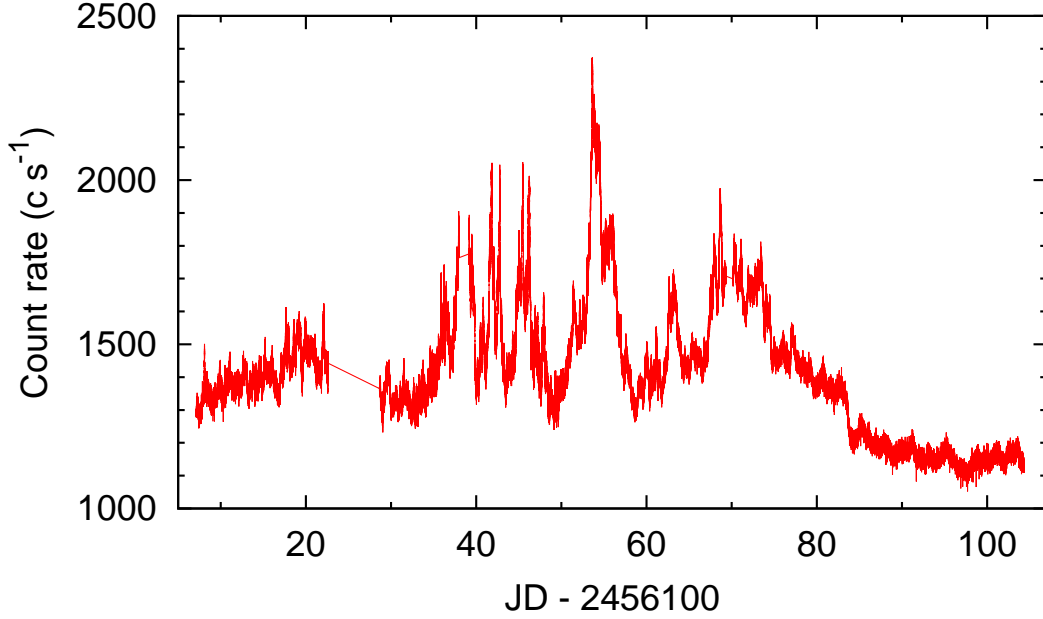


FIG. 1: Light curves obtained by *Kepler* spacecraft in Quarter 14. The object monitored for 100 d with one-minute time resolution.

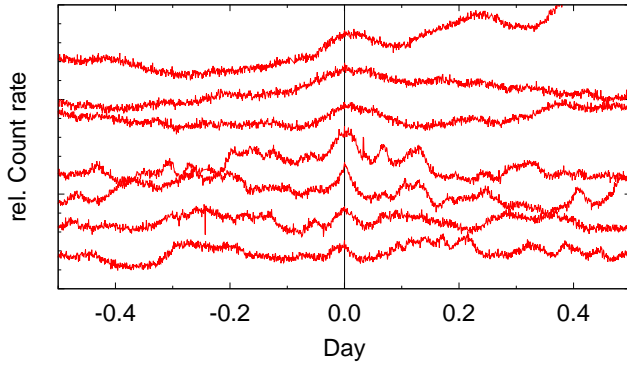


FIG. 2: Examples of rapid variations. These variations are ranged with reference to peak times of individual extrema during the period of rapid variations. From bottom to top, the peak times of rapid variations are JD 2456134.84, 2456147.23, 2456147.91, 2456151.40, 2456152.15, and 2456153.04, respectively.

mean profile within  $\pm 1$  day, and calculate standard deviations in each time bin. The standard deviations of normalized mean profiles can be regarded as the systematic uncertainties associated with the sampling of shots. The bottom panel of figure 3 shows calculated standard deviations. These deviations are rang-

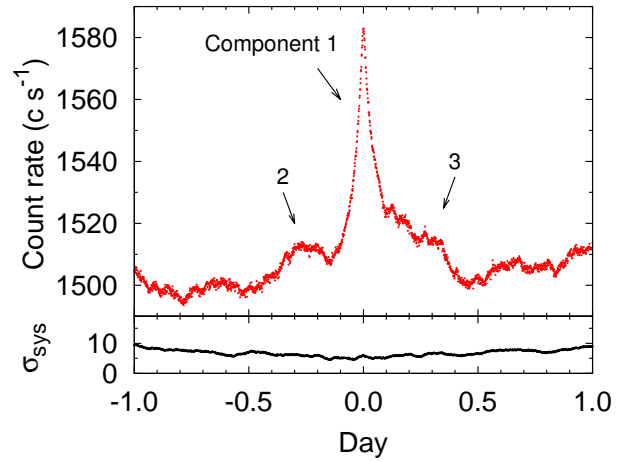


FIG. 3: A mean profile of detected shots. Upper panel shows the mean profile of shots and bottom panel shows the standard deviation estimated from a non-parametric bootstrap method. See text for detail.

ing from 6 to 10 count  $s^{-1}$ . Detected components from 1 to 3 in the mean profile of shots can be regarded as the real phenomena, not the artificial ones caused by the systematic uncertainty of the sampling of shots.

Component 1 reflects general features of shots directly, because this component is distributed around the peak time. First, we apply this exponential shape of component 1 to a function proposed by Abdo et al.;

$$F(t) = F_0 [e^{-t/T'_r} + e^{t/T'_d}]^{-1} + F_c, \quad (1)$$

where  $T'_r$  and  $T'_d$  are variation timescales of rise and decay phases,  $F_c$  represents a constant level underlying the component 1, and  $F_0$  measures the amplitude of the shot [1]. We evaluate its goodness of fit by  $\chi^2$  test,  $\chi^2 = \sum \{F_{\text{data}}(t_i) - F_{\text{model}}(t_i)\}^2$ . The  $\chi^2$  of the best fitted function is 2278 within  $\pm 0.1$  day of the mean profile to except contaminations of other components. On the other hand, we apply an another function;

$$F(t) = \begin{cases} F_0 e^{-t/T_r} + F_c, & t < 0 \\ F_0 e^{t/T_d} + F_c, & t > 0, \end{cases} \quad (2)$$

where  $T_r$  and  $T_d$  are e-folding times of rise and decay, and  $F_c$  and  $F_0$  are the same in the case of function (1). We also calculated the  $\chi^2$  of this function,  $\chi^2=469$ . Figure 4 shows the applied functions with the best fitted parameters superposed on the mean profile and its residuals. Although the function (1) shows obvious residuals during the peak time in panels "a" and "b" of figure 4, the residuals in the case of function (2) are suppressed shown in panels "c" and "d". This indicates that the mean profile is more spiky than the expected profile from function (1). Therefore, the goodness of fit of the function (2) is more plausible than that of function (1) to represent the component 1 of the mean profile.

We estimated the best-fitted parameters with a chi-squared test. The mean profile, however, has a systematic uncertainty caused by the sampling of shots as mentioned above. We applied the non-parametric bootstrap approach to calculate the confidence level with the same way to estimate the errors of calculated parameters. First, we calculated 10000 pseudo mean profiles estimated from resamples with replacement from detected shots. We calculated the best-fitted parameters against individual pseudo profiles, and estimated the confidence levels in these parameters. In table 1, we show the best-fitted parameters of function (2) to the mean profile and the ranges of 95 % confidence levels. We applied the Wilcoxon rank-sum test which was a non-parametric significance test (also referred to as the Mann-Whitney U-test) to the distributions of  $T_r$  and  $T_d$  calculated by the bootstrap approach [15, 25]. We confirmed the difference between the  $T_r$  and  $T_d$ , because the p-value was less than  $10^{-15}$ . Therefore, the component 1 in the mean profile of shots has an asymmetric profile.

TABLE I: Parameters of best-fitted function (2) to component 1 of the mean profile of shots

	Best value	95% confidence level
$T_r$ (day)	0.0416	[0.0320, 0.0543]
$T_d$ (day)	0.0588	[0.0399, 0.0919]
$F_0$ (count s <sup>-1</sup> )	76	[65, 88]
$F_c$ (count s <sup>-1</sup> )	1508	[1484, 1537]

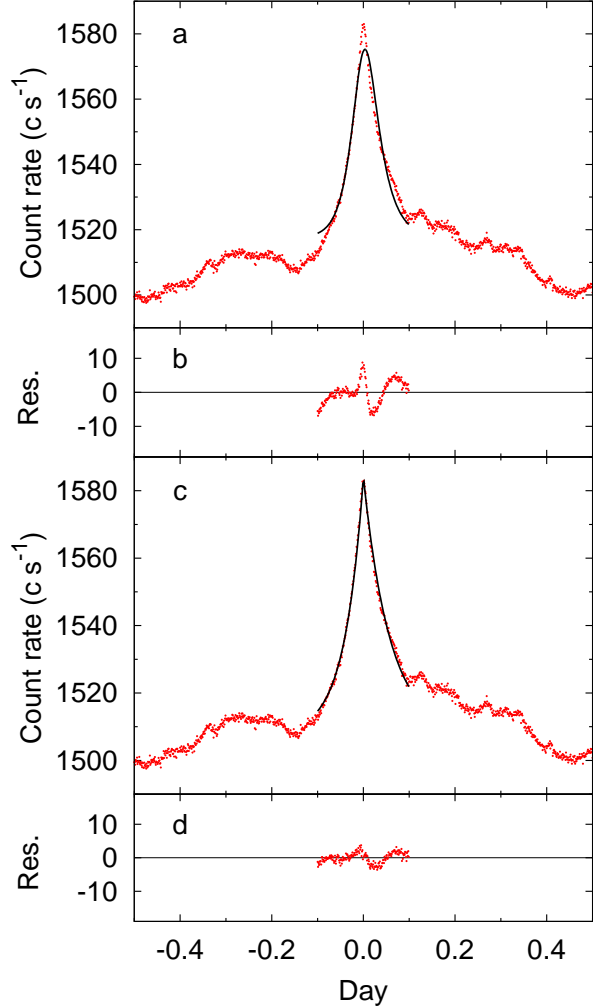


FIG. 4: Best-fitted functions superposed on mean profiles of shots. Panels "a" and "c" show a mean profile of shots and the best-fitted functions (1) and (2). Panels "b" and "d" show residuals between the mean profiles and the estimated best-fitted functions.

#### IV. DISCUSSION

We obtained the optical continuous light curve of blazar W2R 19426+42 with one-minute time resolution by *Kepler* spacecraft. The object showed violent variability and a lot of rapid variations with timescales

less than a day. We detected 195 rapid variations as shots of which amplitude were larger than  $4\sigma$  after subtracting these baseline components, and applied to the shot analysis. The mean profile produced from detected shots shows three components, one fast-spiky (component 1) and two slow-varying components. Component 1 shows an asymmetric profile, faster-rise and slower-decay features with the spiky but smooth-connected peak.

It is poorly understood whether rapid variations are intrinsic phenomena or apparent one caused by a geometrical changing in the jet. There are several models that flux variations are explained as apparent brightness variations, for example varying the Doppler factor for changing the viewing angle [24] or gravitational lensing effect [8]. These models, however, expect that the averaged variation profile is almost symmetric in a simple situation, because the Doppler factor should be changed symmetrically in the averaged variation. In other words, the rise and decay timescales should be equal. Estimated rise and decay timescales of rapid variations, however, are different described in section 3. Thus, these models can be ruled out in the case of rapid variations. Thus, rapid variations may come from authentic phenomena. It is plausible that there is a particle acceleration during the rapid variation, and then, higher-energy particles increase in the emitting region of the variation.

The synchrotron cooling timescale  $\tau_{\text{syn}}$  is represented as,  $\tau_{\text{syn}} \sim 3.2 \times 10^4 B^{-3/2} E^{-1/2} \delta^{-1/2}$  sec, where  $B$  is a strength of magnetic field,  $E$  is an observed energy band, and  $\delta$  is the Doppler factor [21, 23]. If the dissipation of high-energy particles in rapid variations is caused by the synchrotron cooling,  $\tau_{\text{syn}}$  in the rest frame can be represented using the decaying timescale  $T_d$ ,  $\tau_{\text{syn}} = \delta T_d / (1 + z)$ . We estimate  $\delta$  of 5.8

from observed  $T_d$  of the mean profile of shots, where  $E$  is 2.25 eV and assuming  $B$  as 0.5 G which is typical value among the gamma-ray detected BL Lac objects [11]. The mean profile reflects common features of rapid variations. Thus, the estimated  $\delta$  should be a typical value of inner regions where rapid variations happen.

## V. CONCLUSION

The optical continuous light curve with one-minute time sampling obtained by *Kepler* revealed that the mean profile of rapid variations almost showed exponential rise and decay. Rise and decay timescales of shot profile, however, are different, and the profile shows asymmetric profile. A particle acceleration process can produce this asymmetric variations. There are several scenarios which can explain the particle-acceleration mechanism causing the rapid variations; shock-in-jet scenario [16], magnetic reconnection scenario [12]. The shot analysis is also feasible to study the spectral feature of variations, because of large signal-to-noise ratio. Unfortunately, *Kepler* performed only one-band monitoring. Spectral and further observational studies are needed to completely understand the mechanism of rapid variations.

## Acknowledgments

This work was supported by a Grant-in-Aid for JSPS Fellows.

- 
- [1] Abdo, A. A., et al. 2010, ApJ, 722, 520
  - [2] Abdo, A. A., et al. 2011, ApJ, 733, L26
  - [3] Aharonian, F., et al. 2007, ApJ, 664, L71
  - [4] Antonucci, R. 1993, ARA&A, 31, 473
  - [5] Blandford, R. D. & Königl, A. 1979, ApJ, 232, 34
  - [6] Borucki, W., et al. 2010, Sci, 327, 977
  - [7] Carini, M., Miller, H. R., & Goodrich, B. D. 1990, AJ, 100, 347
  - [8] Chang, K., & Refsdal, S. 1979, Nature, 282, 561
  - [9] Edelson, R., & Malkan, M. 2012, ApJ, 751, 52
  - [10] Edelson, R., et al. 2013, ApJ, 766, 16
  - [11] Ghisellini, G., et al. 2010, MNRAS, 402, 497
  - [12] Giannios, D., Uzdensky, D. A., & Begelman, M. C. 2009, MNRAS, 395, L29
  - [13] Jenkins, J., et al. 2010, ApJ, 713, L87
  - [14] Kataoka, J., et al. 2001, ApJ, 560, 659
  - [15] Mann, H. B., & Whitney, D. R. 1947, Annals of Mathematical Statistics, 18, 50
  - [16] Marscher, A. P., & Gear, W. K. 1985, ApJ, 298, 114
  - [17] Nalewajko, K. 2013, MNRAS, 430, 1324
  - [18] Negoro, H., Miyamoto, S., & Kitamoto, S. 1994, ApJ, 423, L127
  - [19] Quirrenbach, A., et al. 1992, A&A, 258, 279
  - [20] Sasada, M., et al. 2008, PASJ, 60, 37
  - [21] Sasada, M., et al. 2010, PASJ, 62, 645
  - [22] Saito, S., Stawarz, L., Tanaka, Y. T., Takahashi, T., Madejski, G., & D'Ammando, F. 2013, ApJ, 766, L11
  - [23] Tashiro, M., et al. 1995, PASJ, 47, 131
  - [24] Villata, M., & Raiteri, C., M. 1999, A&A, 347, 30
  - [25] Wilcoxon, F. 1945, Biometrics Bulletin, 1, 80